Continuous free-crab gaits for hexapod robots on a natural terrain with forbidden zones: An application to humanitarian demining

J. Estremera[a], J.A. Cobano[a] and P. Gonzalez de Santos [a]

[Author vitae]

[a] Department of Automatic Control, Institute of Industrial Automation - CSIC Ctra. Campo Real, Km 0,200 28500 Arganda del Rey, Madrid, Spain

Received 16 September 2008;
revised 31 October 2009;
accepted 17 November 2009.
Available online 22 November 2009.

Abstract

Autonomous robots are leaving the laboratories to master new outdoor applications, and walking robots in particular have already shown their potential advantages in these environments, especially on a natural terrain. Gait generation is the key to success in the negotiation of natural terrain with legged robots; however, most of the algorithms devised for hexapods have been tested under laboratory conditions. This paper presents the development of crab and turning gaits for hexapod robots on a natural terrain characterized by containing uneven ground and forbidden zones. The gaits we have developed rely on two empirical rules that derive three control modules that have been tested both under simulation and by experiment. The geometrical model of the SILO-6 walking robot has been used for simulation purposes, while the real SILO-6 walking robot has been used in the experiments. This robot was built as a mobile platform for a sensory system to detect and locate antipersonnel landmines in humanitarian demining missions.

Keywords: Walking robots; Legged robots; Gait generation; Gait planning

Article Outline

1. Introduction

Mobile robots meet their most demanding scenarios in natural environments, where several difficulties stemming from the unknown, unstructured surroundings combine with different features of the natural terrain that jeopardize robot support. Locomotion can be a problem there, due to terrain conditions (soft ground, slippery terrain) and due to extreme topology, which can merge severe irregularities with areas where a robot can find no support, such as holes and high protrusions.

To achieve complex tasks successfully in these kinds of environment, a mobile robot has to plan its actions at different hierarchical control levels, ranging from the levels that construct the general strategy for accomplishing the task to the levels that decide the actuator's elementary motions. This last planning level, almost trivial in the case of traditional tracked or wheeled robots, is of paramount importance in the case of walking robots and is known as gait generation. To make a robot walk in the desired direction, achieving terrain adaptability and keeping stability, is a very complex task. Leg motion planning will be even more complex if some areas of the terrain cannot provide support, that is, if there are some small zones where feet cannot be placed. These areas are known as forbidden zones. They may be holes, high protrusions or antipersonnel land mines, to give just a few examples. Finally, the robot must know what its position and orientation in a given reference frame are at any time, a problem known as robot localization. There are different techniques for robot localization outdoors that provide differing degrees of accuracy [1] and [2]. In the case of robot localization for humanitarian demining missions, an accuracy of about a few centimeters is required, which dramatically determines which localization technique can be used for this particular application [3] and [4].

Generally speaking, a gait is a sequence of foot movements by which an animal moves forward. In early walking-robot research, gait sequences were inspired by nature, but gradually other ideas based on engineering principles were introduced and proved to have some attractive features.

There is a large number of scientific and technical articles on gait generation for walking robots. Most of them solve the problem under ideal conditions: flat terrain,

precise geometric models, etc. Gaits for irregular terrain have been derived as extensions of and corrections to the gaits formulated for ideal conditions [5] and [6]. This article, on the contrary, introduces a new gait algorithm for hexapod robots capable of walking at a continuous speed (continuous gait) on irregular terrain containing forbidden zones. This new method was designed to solve the problems stemming from the real-life application of legged robots to detect and locate antipersonnel land mines in humanitarian activities [7], [8], [9] and [26].

There are also other gaits, such as wave gaits, which are observed in mammals, reptiles and insects at low speed [10] and [11], crab gaits [12] and [6] and turning gaits, which can be divided into circling and spinning gaits.

Over the last two decades, some researchers have developed many different gaits for hexapod robots capable of avoiding forbidden zones, gaits for adapting to irregular terrain, crab and circling gaits, etc.; however, there is no single gait that combines all these features. Such a gait is, therefore, the main objective of our work.

Free gaits have been developed relying on different techniques: heuristic rules [13], [14], [15] and [16], search graphs [17], [18], [19] and [20], central pattern generators [21] and [22], learning methods [23], and biological studies of insects [24] and [25], just to mention a few examples. However, to date none of these methods has shown full effectiveness and efficiency at controlling a legged robot in unstructured environments. Thus, we propose in this article a new method, which relies on heuristic rules, because these rules are the only ones that can plan leg motions accurately and guarantee stability using physical laws. This method can be applied in general to hexapods; however, it has been particularized for humanitarian demining tasks because it is focused on practical cases with forbidden zones.

To accomplish our main objective, this article first discusses crab gaits, in Section 2. Section 3 describes the new gait planner for hexapods on a natural terrain. Section 4 defines turning gaits for irregular terrain. All these gaits have been assessed in simulation and through experiment, as illustrated in Section 5. Finally, Section 6 presents the discussion and final conclusions.

2. A free-crab gait for hexapod robots

This section presents a new gait for hexapod robots or, in other words, the algorithms to determine which leg motions a walking robot must perform to produce stable locomotion in the desired direction. The gait module is the most characteristic and distinctive level of a walking robot, and it is in charge of dealing with the robot's motion. The actions involved are trivial in traditional vehicles. For instance, the kinematic model of wheeled or tracked vehicles is very simple, as is the relationship between actuator motions and vehicle motions. On the other hand, the kinematic model of a walking robot can be highly complex, and a large number of actuators has to be coordinated for the robot to move efficiently. Furthermore, the stability of a wheeled robot is accomplished passively for a range of terrain conditions (terrain inclination, for instance), while a walking robot must guarantee its stability actively by using its control system. Finally, and this is of huge importance, wheeled robots do not posses the kinematic limitations legged robots do. These limitations force a legged robot to alternate between different states: the support phase to support and propel the body, and

the transfer phase to recover the initial state so the body can enjoy continued support. The gait generator is in charge of all these actions, but it is also the module responsible for all the features that make a walking robot superior to traditional vehicles, i.e., omni-directionality, adaptability to very irregular terrain and the ability to walk over terrain containing forbidden zones.

The method presented herein is a general method for hexapod robots; however, the simulations and experiments presented in Section 5 have been tailored for the SILO-6 robot model (see Fig. 1) [8], [9] and [26]. This robot has been designed to meet the requirements of detecting and locating antipersonnel landmines in humanitarian missions: mobility over forbidden zones (land mines), adaptability to very irregular terrain (natural environments) and ability to follow predefined trajectories with high accuracy. Table 1 presents some of the kinematic parameters defined in Fig. 2 and general features of the SILO-6 walking robot.

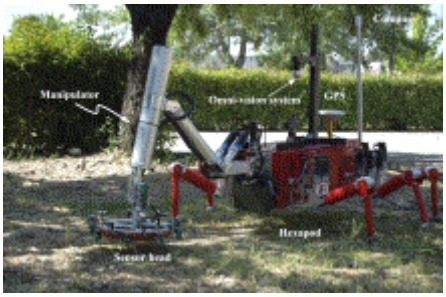

Full-size image (66K)

Fig. 1.

The SILO-6 walking robot.

Table 1. Features of the SILO-6 walking robot.

Body	Dimensions	Length (L_B)	0.88 m
		Width (W_B)	0.63 m
		Height (H_B)	0.26 m
		Stroke pitch (P_x)	0.365 m
	Mass		28.2 kg
Leg	Link length	a_1	0.084 m
		a_2	0.250 m
		a_3	0.250 m
	Stroke (R_x)	0.25 m	
	Mass	4.3 kg	
	Foot speed	Transfer phase	0.140 m/s

		Support phase	0.05
Robot	Total mass	54 kg	
	Position accuracy (with DGPS)	±0.02 m	
	Clearance (Maximum height of irregularities)	0.35 m	
	Speed	0.05 m/s	

The kinematic parameters are defined in Fig. 2.

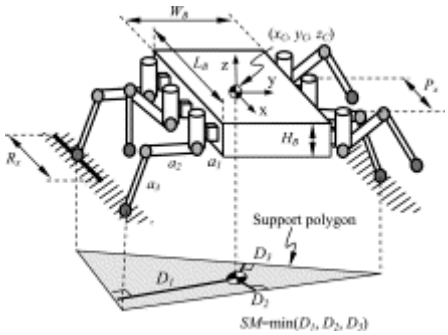

Full-size image (39K)

Fig. 2.

Support polygon and stability measurements.

2.1. General approach to gait definition

In humanitarian missions, a legged robot might perform a periodic gait, which can be implemented easily and efficiently. However, when there are forbidden zones involved, the periodic gait can be very difficult to maintain. In such a case, it is best to use a gait that can move any leg at any time, that is, one that is not forced to maintain a periodic leg motion sequence. These gaits, as mentioned above, are known as free gaits.

A preliminary selection of foot liftings and footholds has been based on that of the alternating tripod gait. The alternating tripod gait can achieve the theoretical maximum speed for a hexapod, and it is also the optimum gait from the stability standpoint. These are the main advantages for our application, bearing in mind that statically stable walking robots are intrinsically slow vehicles, and we are dealing with a real application on irregular terrain in which we must ensure vehicle stability. Furthermore, this method drastically limits the large number of different solutions available when planning the leg motions of a six-legged robot. Using a gait based on alternating tripods, we can greatly simplify the foot-lifting instants and foothold instants, while the leg sequence becomes trivial.

Our algorithm must meet two additional requirements regarding adaptation to an irregular terrain:

1. The robot must be capable of adapting to an irregular terrain without previous knowledge of the terrain, and

2. The gait must be capable of using the information provided by stereoceptive sensors, when available, to improve terrain adaptation. In the experiments presented below, this terrain information is made available by a sensor head fixed in the front of the mobile robot that informs the controller about the position of potential landmine alarms (see

Fig. 1
).

This last requirement includes the possibility of planning foothold searches in terrain including forbidden zones.

Taking into account our current application, the gait must be also capable of following trajectories accurately. Thus, the gait should guarantee that the center of gravity (*COG*) of the body follows the trajectory indicated by a higher control level. This feature should not be changed to improve other features, such as stability. Additionally, in order to facilitate the following of trajectories, we have designed both crab and turning gaits.

Finally, the optimization of stability and speed has been considered a general criterion for gait design. This is of vital importance in searching for footholds, where a compromise between both gait features is a vital necessity.

As mentioned in Section 1, our gait is based on two heuristic rules that define:

1. The instant of foot liftings

2. The new footholds.

Some geometric and kinetic calculations are also required to define the gait. Thus, the gait planner is divided into three modules:

1. Foot-lifting planner

2. Body motion planner

3. Foothold planner.

These modules are presented in the following sections.

2.2. Achieving gait stability

Gait stability is studied assuming that the legs of the robot are grouped into two tripods, each one formed by the front and rear leg of one side and the central leg of the opposite side. Subscripts *F*, *C*, and *R* denote the front, center and rear leg, respectively, in a tripod (see Fig. 3). During locomotion the tripod can be in support (stand) or in transfer (swing). Both tripods can be simultaneously in support, but they will never be in transfer at the same time.

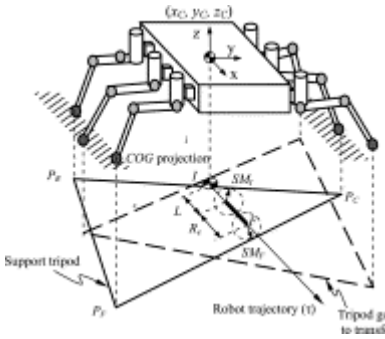

Full-size image (47K)

Fig. 3.

Definition of gait parameters.

Henceforth we will use the term “tripod” interchangeably to denote both the legs and the footholds of a given tripod. For the computation of stability measurements, we will consider that the body is level and the body’s *COG* lies at the body’s geometric center. To formulate the gait algorithm we define the following magnitudes related with robot stability.

Definition 1

The stability margin, *SM*, also known as the absolute static stability margin, is the smallest distance from the vertical projection of the *COG* on a horizontal plane to the sides of the support polygon formed by joining the projections of the footholds on the same horizontal plane (see Fig. 2).

Definition 2

The minimum absolute stability margin, $SM_{\min}$, is the smallest allowed *SM* value. This is a value to guarantee stability in spite of body level errors, leg acceleration, flexion in links, backlash in joints, etc.

Definition 3

The transfer starting point, $\underline{I}$, and the transfer final point, $\underline{F}$, are defined in the following terms:

Let us assume a tripod placed at points $\underline{P_F}$, $\underline{P_C}$,$\underline{P_R}$, a tripod that is going to be transferred, and let us assume $\underline{R_e}$ to be the distance the body is going to move during the transfer phase. Then, the transfer starting point $\underline{I(P_F,P_C,P_R,R_e)}$ and the transfer final point $\underline{F(P_F,P_C,P_R,R_e)}$ are defined to satisfy the following conditions:

Condition 1.1: Points I and F must lie on trajectory τ (see Fig. 3). That is:

(1) $I(P_F, P_C, P_R, R_e) \in \tau$
$F(P_F, P_C, P_R, R_e) \in \tau$ where τ is the trajectory to be followed by the robot.

Condition 1.2: The distance between points I and F must be R_e. That is:

(2) $\delta_{PP}(I(P_F,P_C,P_R,R_e),F(P_F,P_C,P_R,R_e))=R_e$ where $\delta_{PP}(m,n)$ is the Euclidian distance between points m and n.

Condition 1.3: The distance from point I to line P_RP_C and the distance from point F to line P_FP_C must be equal (see Fig. 3). That is:

(3) $\delta_{PL}(I(P_F,P_C,P_R,R_e),P_RP_C)=\delta_{PL}(F(P_F,P_C,P_R,R_e),P_FP_C)$ where $\delta_{PL}(p,mn)$ is the distance from point p to the straight line passing through points m and n.

If the transfer phase starts when the *COG* is over $I(P_F,P_C,P_R,R_e)$, and during the transfer phase the body moves by about R_e, then the stability margin is the largest during the transfer phase. Note that the defined distances and points are indeed projections onto a level plane (see Fig. 3); therefore, the terrain irregularities do not influence to compute $I(P_F,P_C,P_R,R_e)$ and $F(P_F,P_C,P_R,R_e)$. The same can be applied to the forbidden zones that are detected in advance by the sensor head (out of the scope of this paper) and avoided as footholds.

Definition 4

The distance to the leg transfer starting point, L, is defined as:

(4) $L(P_F,P_C,P_R,R_e)=\delta_{PP}(COG,I(P_F,P_C,P_R,R_e))$. That is, L is the distance the *COG* must travel to reach the transfer starting point, $I(P_F,P_C,P_R,R_e)$. Let us assume a support tripod located at points P_F,P_C,P_R, and a tripod ready to execute the leg transfer phase; then, $L(P_F,P_C,P_R,R_e)$ is the distance that the body must travel before the starting instant of the transfer phase in order to guarantee that the stability margin during the transfer phase is the maximum. Note that we have assumed that the body moves by about R_e during the transfer phase.

Definition 5

The transfer stability margin, $SM_t(P_F, P_C, P_R, R_e)$, is defined as the following distance:

(5) $SM_t(P_F, P_C, P_R, R_e) = \delta_{PL}(I(P_F, P_C, P_R, R_e), P_C P_R)$. Alternatively, it can be defined as:

(6) $SM_t(P_F, P_C, P_R, R_e) = \delta_{PL}(F(P_F, P_C, P_R, R_e), P_F P_C)$ because by definition both distances are equal. That is, SM_t is the absolute stability margin at the beginning and

ending of a transfer phase in which the body travels by about R_e, and the transfer phase starts at such a point that the stability margin is the largest.

2.3. Foot transfer trajectories

The shape of the foot trajectory in a transfer phase determines certain aspects of foothold and foot-lifting planning; hence, it is important to define the foot trajectory properly. The foot transfer trajectory used to move a foot from a foothold P_o to a foothold P'_o consists of three subphases, each of which performs a theoretic straight-line trajectory (see [Fig. 4] and [Fig. 5]). These subphases are:

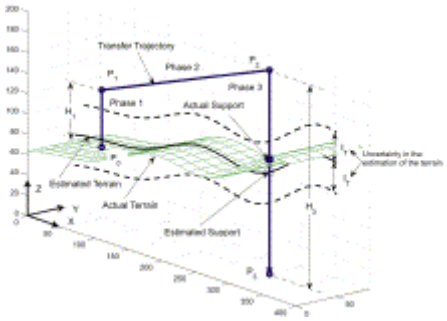

Full-size image (60K)

Fig. 4.

Foot transfer theoretic trajectory in the world reference frame.

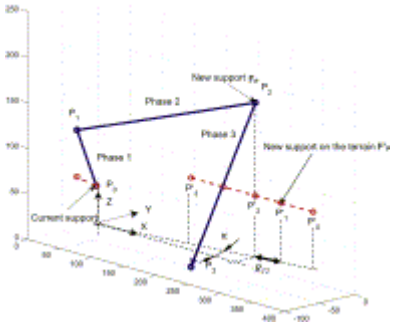

Full-size image (53K)

Fig. 5.

Foot transfer theoretic trajectory in the body reference frame.

Subphase 1: In this subphase the foot rises from its foothold up to a height H_1 following a straight, vertical theoretic trajectory in the world reference frame (see Fig. 4). The value of H_1 is fixed in such a way that the foot in transfer lifts from the ground sufficiently. The foot will move at the average-horizontal body speed V_{BH} and at an average-vertical body speed V_V with respect to the body reference frame (see Fig. 5). In general, during this subphase the body moves a distance R_1. That is:

$$R_1 = \frac{V_{BH} H_1}{V_1}. \quad (7)$$

Note that Fig. 4 plots the leg trajectory in the world reference frame and Fig. 5 plots the same trajectory in the robot reference frame, that is, Fig. 5 is the trajectory seen by an observer onboard the robot.

Subphase 2: In this subphase the body moves up to point P_2, whose components are the x- and y-components of the foothold and whose z-component is a distance $H_3/2$ of the initial ground-height estimation. Note that $H_3/2 > I_T$, where I_T is the uncertainty over the ground height (see Fig. 4). The foot moves in a theoretic straight line, in the world reference frame, from the final point of subphase 1, P_1, to a point F computed by the foothold planner. This trajectory forms an angle α with the x-axis of the body reference frame. The average speed of this motion, $v=(v_x,v_y,v_z)^T$, is given by:

$$\begin{aligned} v_x &= V_2 \\ v_y &= \frac{(P_{1y} - F_y) V_2}{(P_{1x} - F_x)} \\ v_z &= \frac{(P_{1z} - F_z) V_2}{(P_{1x} - F_x)}. \end{aligned} \quad (8)$$

The distance traveled by the body during this subphase is R_2, given by:

$$R_2(F) = \frac{V_{BH}(P_{1x} - F_x)}{V_2}. \quad (9)$$

Subphase 3: In this subphase the foot moves down vertically in the world reference frame until foot-ground contact is eventually detected. This motion is stopped when the distance traveled is greater than a given distance H_3, which is at least twice the uncertainty of the ground height, I_T. The foot in transfer moves at an average-horizontal speed V_{BH} and an average-vertical speed V_3, in the body reference frame (see [Fig. 4] and [Fig. 5]). We define R_3 as the distance that the body travels during the whole subphase, assuming the foot does not contact with the ground and travels H_3. Therefore:

$$R_3 = \frac{V_{BH} H_3}{V_3}. \quad (10)$$

The foot motion stops if it reaches the boundary of its workspace. In that case, the subphase is also finished. If the subphase finishes and the foot is not in contact with the ground, the transfer phase fails. Note that the foot trajectory of every subphase is defined as a straight line followed at a given average speed; however, in order to avoid dynamic effects each trajectory has its acceleration/deceleration phases. In the gait algorithm, we are interested in computing foot strokes and foot travel times; therefore, we use trajectory lengths and average speeds and the instant speeds are computed by the leg joint controllers.

The legs always perform the transfer phase grouped in tripods and in a synchronized fashion. The legs in a tripod start subphase 1 of the transfer phase when instructed to do so by the foot-lifting planner. All the legs in a tripod must start subphase 2 simultaneously; therefore, a leg will stop at the end of subphase 1 if any of the other

legs have not finished the subphase. The same procedure is applied to accomplish subphase 3 in a synchronized fashion. With this method, we guarantee that the relative position of the footholds does not depend on the leg transfer time. The transfer of a tripod finishes when all of the legs have contacted the ground. Note that Fig. 5 plots the points P_i', that define the estimated foothold when the foot is at point P_i. The foothold is a fixed point in the terrain; therefore, it moves backwards when the robot moves forward.

2.4. Gait parameters

After the leg transfer trajectories of a tripod have been defined, the following definitions are required to formulate the gait.

Definition 6

$R_{T2}(P_F,P_C,P_R)$ is the distance that the body moves while the legs complete subphase 2 of their transfer phase to foothold tripod (P_F,P_C,P_R). That is:

(11)$R_{T2}(P_F,P_C,P_R)=\max(R_2(P_F),R_2(P_C),R_2(P_R))$. In other words, for the legs of a tripod that start each transfer phase in a synchronized fashion, R_{T2} is given by the leg in the tripod that needs the longest time to complete transfer subphase 2. Note that the body moves forwards the same distance that the feet move backwards, and the foot motions can be obtained through the joint encoder readings.

Definition 7

$R(P_F,P_C,P_R)$ is the distance that the body moves while completing the leg transfer phase to foothold tripod (P_F,P_C,P_R):

(12)$R(P_F,P_C,P_R)=R_1+R_{T2}(P_F,P_C,P_R)+R_3$.Due to the uncertainty of the terrain height, the body will travel a distance shorter than or equal to $R(P_F,P_C,P_R)$, depending on the height of the feet.

Definition 8

The reduced kinematic margin, $K(P)$, of a point P belonging to a foot workspace is defined as:

(13)$K(P)=\xi-R_1$ where ξ is the distance that P can be moved in the opposite direction to the vehicle motion before leaving the foot workspace (see Fig. 6).

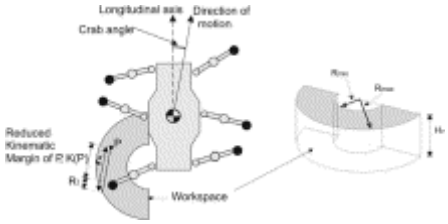

Full-size image (24K)

Fig. 6.

Reduced kinematic margin and leg workspace.

Note that if $K(P)>0$, a leg placed at P can complete transfer subphase 1 (i.e., can be lifted) without leaving the leg workspace. During this subphase the body will move by about R_1.

Definition 9

The reduced kinematic margin of a tripod $K(P_F,P_C,P_R)$ is the smaller reduced kinematic margin of the foothold (P_F,P_C,P_R) of a tripod. That is:

(14) $$K(P_F,P_C,P_R)=\min(K(P_F),K(P_C),K(P_R)).$$

Definition 10

The robot's reduced kinematic margin, K_R, is the smaller reduced kinematic margin of the tripod in support. Therefore, the tripod in transfer is not considered in computing this magnitude:

(15) $$K_R = \begin{cases} \min(K(P_F), K(P_C), K(P_R), K(Q_F), K(Q_C), K(Q_R)) : \\ \quad \text{for two tripods in support at } (P_F, P_C, P_R) \text{ and} \\ \quad (Q_F, Q_C, Q_R) \\ \min(K(P_F), K(P_C), K(P_R)) : \\ \quad \text{for a tripod in support at } (P_F, P_C, P_R). \end{cases}$$

3. Gait planner

As mentioned in Section 2.1, the gait planner is divided into a foot-lifting planner, a body motion planner and a foothold planner.

3.1. Foot-lifting planner

The maximization of the kinematic margin is a criterion used intensively to design gaits for walking robots. This criterion just gives the vehicle's capability of moving in the desired direction taking the kinematic limitations into account, and it states that the leg

to be lifted is the one that has the smallest reduced kinematic margin, because it is the closest to the boundaries of the foot workspace and thus limits the motion of the robot.

Another criterion to be taken into account in planning leg liftings is the maximization of the stability margin. The smallest stability margin is obtained during the period in which the vehicle has one tripod in support and the other one in transfer. Thus, it is important to plan accurately the instants in which the transferences start to maximize the stability margins. Taking into account these considerations and the previous definitions, the foot-lifting planner will be based on the following rules and will act when both tripods are in support.

Foot-lifting condition 1: The tripod with the smaller reduced kinematic margin must start its transfer phase when $\underline{L(P_F,P_C,P_R,R_e)=0}$.

Foot-lifting condition 2: The tripod with the smaller reduced kinematic margin must start its transfer phase if its reduced kinematic margin vanishes, if and only if $SM > SM_{\min}$.

Note that if the distance traveled by the robot is different from the distance assumed a priori (for instance, if the transfer phase lasts more than the assumed time or the body velocity is changed), the stability will not be the best, i.e., the largest stability margin considered in Section 2.2. In this case, $\underline{R_e}$ must be determined by estimating a typical time for the transfer phase. This time and the body average speed will determine $\underline{R_e}$. Additionally, as indicated in Section 3.3, the foothold search is run to guarantee that the body travels a distance smaller than or equal to $\underline{R_e}$.

3.2. Body motion planner

The motion of the body is defined in many aspects by the human operator or the control level in charge of steering the robot. However, other aspects are determined automatically to adapt the robot to unstructured environments. The parameters that define body motion and the methods used to obtain the true values are presented below.

Crab angle ($\underline{\alpha}$): This is the angle between the longitudinal axis of the robot's body and the robot's direction of motion. This parameter defines the lateral motions of the body. The module in charge of robot steering can vary this value to control the tracking trajectory error.

Horizontal body speed (V_{BH}): This is the robot's body average speed in the direction given by the crab angle, $\underline{\alpha}$. We assume that a module in a higher control level determines a nominal speed, V_{BH}, as a function of the task. Thus, the body moves forwards at a default average speed $V_{BH} = V_{BHN}$. However, the controller can stop the motion (i.e. the controller can set $V_{BH} = 0$) in the following cases:

1. If $SM \leq SM_{\min}$, that is, the robot stability is smaller than the minimum allowed.

2. If $\underline{K \leq 0}$, that is, if a foot in support is about to reach a foot workspace boundary.

3. If not all feet in a tripod are in contact with the ground at the end of subphase 3 of the tripod transfer phase.

Vertical body speed (V_{BV}): This speed varies automatically to adapt to the terrain. The average foot height in support, Z_{pm}, is controlled to keep its value around a preset value, H_m. The vertical body speed varies according a proportional control law:

(16) $V_{BV} = Kp_{vv}(H_m - Z_m)$ where Kp_{vv} is the controller gain tuned experimentally. This law is applied if the feet are inside their workspace. Otherwise, the controller applies $V_{BV} = 0$.

Body pitch speed (ω_{BP}) *and body roll speed* (ω_{BR}): These magnitudes are determined automatically to keep the body horizontal. They are computed as a function of the body pitch angle, ϕ, and the body roll angle, θ (given by a couple of inclinometers located in the robot's body), as well as the footholds of the feet in support using the following simple control laws:

(17) $\omega_{BP} = -Kp_{\varphi}\varphi$
$\omega_{BR} = -Kp_{\theta}\theta$ where Kp_{ϕ} and Kp_{θ} are the controller gains. As with vertical body speed, these control laws are used if and only if the feet are inside their workspaces. Otherwise, the controller will command $\omega_{BP} = 0$ and $\omega_{BR} = 0$.

Yaw body speed (ω_{BY}): This speed is fixed by the operator or a higher control level to change the yaw angle of the body.

All these linear and angular average speeds are factored in to compute the instant linear speed of every foot in support. The foot horizontal speed in subphases 1 and 3 is also computed in this fashion.

3.3. Foothold planner

The search for new footholds for a tripod in transfer is performed when the tripod is lifted, i.e., when it has already executed transfer phase 1 and the tripod feet are at points P_1 of the transfer trajectory (see [Fig. 4] and [Fig. 5]). The search is based on proposing three candidate points (F_F,F_C,F_R) where the three legs of the tripod will be moved during transfer phase 2. Each one of these three points corresponds with point P_2 of the transfer trajectory in [Fig. 4] and [Fig. 5]. When a foothold tripod candidate is proposed, it is evaluated with different criteria. This process is repeated for different foothold tripods, and the best one is finally selected. The strategy used to evaluate the footholds has two parts. First, a series of conditions based on concepts such as stability, kinematic limits, etc., is taken into account to classify the footholds as either valid or non-valid. Second, the group of valid footholds will be evaluated using a cost function, which allows two different criteria (stability and maximum speed). The greatest value of this cost function will define the most appropriate foothold tripod to be selected.

3.3.1. Foothold conditions

Given a tripod in support, a tripod in transfer, an estimated distance the body is going to move during the transfer phase, R_e, and a foothold tripod candidate F_F,F_C,F_R for the tripod in transfer (with respect to the body reference frame), the footholds will be valid if they fulfill the following six conditions:

Support condition 1: The footholds must be outside any forbidden zone. To determine if a certain foothold $\underline{F_p}=(\underline{x_p},\underline{y_p})^T$ is a valid point, a point on the terrain, $F'_p = (x'_p, y'_p)^T$, must be calculated. This is the point where the foot will be placed at the end of the transfer phase, which can be expressed in the robot reference frame as (see Fig. 5):

(18) $$F'_P = F_P + \begin{pmatrix}\cos\alpha \\ \sin\alpha\end{pmatrix} R_{T2}(F_F, F_C, F_R).$$

Therefore, F'_F, F'_C and F'_R will be allowed footholds on the terrain.

Support condition 2: From the stability standpoint, the optimal instant to initiate the transfer of the support tripod must come before the instant in which the reduced kinematic margin of the support tripod vanishes. To guarantee this, it is assumed that during the next transfer of the support tripod the body will travel a distance $\underline{R_e}$. This is:

(19) $$\underline{L(F_F,F_C,F_R,R_e)<K(F_F,F_C,F_R)-R_{T2}(F_F,F_C,F_R).}$$

$\underline{L(F_F,F_C,F_R,R_e)}$ is the distance the body moves before starting the following transfer (as described in Definition 4 and because of the foot-lifting condition 2) in order to maximize the static stability, and must be lower than the kinematic margin, $\underline{K(F_F,F_C,F_R)}$. $\underline{R_{T2}(F_F,F_C,F_R)}$ is the motion of the body while the legs move toward the new footholds. Thus, the kinematic margin of the support tripod is reduced in this amount. This condition, hence, guarantees that the support legs are inside their workspaces up to the optimum instant to start the transfer phase.

Support condition 3: The reduced kinematic margin of the new footholds must be large enough so that it does not vanish before the support tripod completes its next transfer. It is assumed that the following transfer of the support tripod will begin at the right instant, from the stability standpoint, in order to impose this condition. Additionally, the body will travel a distance $\underline{R_e}$ during transfer. Therefore, the following condition must be fulfilled:

(20) $$\underline{K(F_F,F_C,F_R)>L(F_F,F_C,F_R,R_e)+R_e.}$$

As mention above, $\underline{L(F_F,F_C,F_R,R_e)}$ is the distance the body moves before starting the following transfer. $\underline{R_e}$ is the distance the body moves during the transfer phase, therefore, the right side of (20) is the distance the body moves before finishing the next transfer. Therefore, this condition tries to maintain the support feet inside their workspaces until the other tripod finishes its transfer phase.

Support condition 4: The transfer tripod will achieve the support phase (in spite of the uncertainty in the elevation of the terrain) before the right instant for lifting the support tripod arrives. Thus, the support tripod can be lifted while stability is maintained. This condition is expressed by means of the following relationship, assuming that body displacement during the transfer is $\underline{R_e}$:

(21) $$\underline{L(F_F,F_C,F_R,R_e)>R_3.}$$

If this condition is not fulfilled, when the transfer tripod touches the ground, the *COG* will be located ahead of the right point for lifting the other tripod, which would then be

necessarily lifted under a non-suitable condition because the foot-lifting condition 1 is not fulfilled (see Section 3.1).

Support condition 5: The stability margin must be greater than a pre-defined minimum $SM_{\min}$ during the following transfer of the support tripod, assuming that the transfer of the support tripod will begin at the right instant from the stability standpoint (as indicated in support condition 2 and in Section 3.1) and that the body displacement is R_e during the transfer. Therefore:

(22) $SM_t(F_D, F_C, F_T, R_e) > SM_{\min}$.

Support condition 6: The body displacement during the tripod transfer must not exceed the R_e value assumed in support conditions 2, 3, 4 and 5. Therefore, the following expression must befulfilled:

(23) $R(F_D,F_C,F_T)<R_e$.

Note that in order to formulate support conditions 2, 3, 4 and 5, the body displacement is assumed to be R_e during subsequent transferences, which may not occur in some cases. On the other hand, support condition 6 demands that during the current transfer phase the body must not travel more than R_e. Therefore, all transferences, including future ones, will fulfill this condition at their computation instant. Thus, the assumption made in support conditions 2, 3, 4 and 5 is consistent.

3.3.2. Criterion for foothold selection

The parameters to be improved in gait design are the stability and maximum speed of the robot. To achieve a high speed, we need to obtain large kinematic margins in order to perform the lowest possible number of leg transfer phases (support condition 3). However, if we select a foothold tripod trying to maximize the kinematic margins only, the stability margin could decrease. Note that if the tripod yields a stability margin below $SM_{\min}$, it will be rejected; however, a foothold tripod with stability margins above but close to $SM_{\min}$ will be allowed.

On the contrary, if we select a tripod trying to maximize the stability margin only, then the kinematic margins could decrease. Note that if a tripod has a kinematic margin below the restriction imposed by support condition 3 it will be rejected, but nothing would prevent selecting a tripod with a kinematic margin close to this limit. With short kinematic margins we need to exert a large number of transfer phases and the robot would be most of the time supported on one tripod. Furthermore, a sudden increase of the commanded body speed could cause the kinematic margin to vanish before than expected, forcing a body stop.

That means we need to balance both contributions. To achieve that trade-off between kinematic margin and stability margin, the foothold tripod candidates that fulfill support conditions 3 and 5, presented in Section 3.3.1, are evaluated according to the following cost function:

(24) $Ev(F_F, F_C, F_R) = K(F_F, F_C, F_R) + k_{ev} SM_t(F_F, F_C, F_R, R_e)$ where k_{ev} is a parameter to weigh the cost function. That is, the foothold is obtained as the foothold tripod

candidate that maximizes (24). The use of k_{ev} is a linear manner of weighing both speed and stability and it is tuned by and experimental trade-off.

3.3.3. Foothold-searching algorithm

To search for new footholds, we define a number N of discrete, finite possible footholds within each leg workspace of the tripod. Fig. 7 illustrates the candidates selected for the SILO-6 leg.

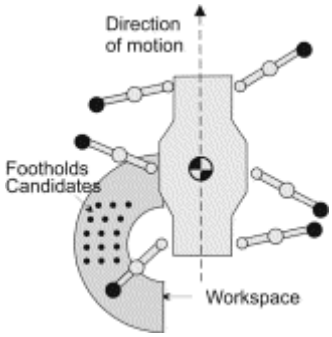

Full-size image (25K)

Fig. 7.

Foothold candidates in foothold planning.

In the next step, all possible support tripods formed with the different combinations of the possible footholds of each leg are analyzed, verifying whether they fulfill all the conditions specified in Section 3.3.1 and evaluating those footholds that are valid according to the criterion for foothold selection defined in Section 3.3.2. If there is more than one valid foothold tripod, the foothold tripod that obtains the greatest E_v will be the new support tripod and the transfer will be completed. Finally, if at least one foot cannot touch the selected footholds, a new forbidden zone will be defined for the footholds and the procedure will be repeated to find a new, different foothold. This is an intensively computing method of evaluation among N evenly-spaced candidates in the workspace for each foot. More effective methods for searching the appropriated candidate can be investigated, but this is outside the scope of this present work. The final value of N is a trade-off between computational burden and robot's speed. In this point, it is worth mentioning that leg transferences in statically stable walking robots are slow and the central computer can be used for solving these types of heavy computational method.

4. Turning gaits

The crab gait generated in this process can be extended into a turning gait in which the robot moves around a given axis. If the rotation radius is large enough to keep stability, we get a circling gait ($V_{BHN} \neq 0$ and $\omega_C \neq 0$). If the rotation radius is null, i.e., the robot turns around its own COG ($V_{BHN} = 0$ and $\omega_C \neq 0$), we get a spinning gait. Both the circling and the spinning gaits are described below.

4.1. Circling gait

To extend the crab gait into a circling gait, all that need be done is to adapt the definitions of robot displacement and foot motion. The angles turned by the body and the legs in support are the same in a circling gait, whereas the distances traveled by each foot and the body are, in general, different. Hence, it is advisable to redefine in angular magnitudes the distances that represent a foot or body displacement in the crab gait. The following considerations must be taken into account in order to formulate the circling gait:

We assume that during transfer subphases 1, 2 and 3, the robot turns certain angles ρ_1, ρ_2, ρ_3, which are equivalent to the distances R_1,R_2 and R_3 of the crab gait. These angles can be calculated in a similar way.

The angular reduced kinematic margin of point P within the leg workspace is defined as:

(25)$K_G(P)=\psi-\rho_1$ where ψ is the angle that point P can turn around the center of rotation in the opposite direction to the turn of the robot before leaving the leg workspace.

The definitions of transfer starting point, transfer final point and distance to the leg transfer starting point (see Section 2.2 and Fig. 3), which relates stability with body displacement, should also be redefined to take into account the new circular trajectory of the *COG*. In addition, the magnitudes representing body displacements (L,R_e) should be redefined as angular displacements around the center of rotation of the trajectory.

Finally, the circular trajectory that follows the point on the terrain (from the body reference frame) must be considered in the computation of footholds, in order to calculate the point at which the foot will be supported at the end of the transfer phase and thus to determine if it is a forbidden zone (support condition 1).

The gait thus defined would behave the same as the crab gait when turning radii are sufficiently large, but it will fail for a range of small turning radii. This is explained below.

4.2. Spinning gait

There is a special feature in spinning gaits: The *COG* does not move, and so stability conditions do not change when the body is moving. Therefore, there is no point in defining the transfer starting point, transfer final point, distance traveled before the leg transfer or distance traveled during the transfer phase. Consequently, foot-lifting condition 1 and support conditions 2, 3, 4, 5 and 6 are not appropriate. Thus, it is necessary to redefine the foot-lifting and support conditions. In circling gaits of small radius, the body displacements are not sufficient to produce appreciable changes in the robot's stability. Therefore, methods similar to those employed in the spinning gait should also be used in these cases.

To formulate the spinning gait, a simplified method for choosing foot liftings is proposed with the following conditions:

Turn lifting condition: A tripod begins its transfer when the other tripod finishes its transfer phase.

Regarding of the foothold search, the following conditions are imposed:

Turn support condition 1: The feet cannot be supported on forbidden zones of the terrain.

Turn support condition 2: The absolute stability margin, *SM*, of the new support tripod must be greater than a pre-defined minimum, $SM_{\min}$.

The stability margin of the new tripod will be the stability margin used throughout the entire subsequent transfer, so it is advisable to make it large enough.

Turn support condition 3: The angular reduced kinematic margin of the new support tripod must be greater than a minimum ρ_e.

Turn support condition 4: The angle that the body turns during the transfer must be smaller than a maximum ρ_e.

The last two conditions jointly guarantee that, while a tripod performs its transfer phase, the tripod in support will not stray from its kinematic limits.

5. Simulation and experimental results

Different simulations and experiments tailored for the SILO-6 walking robot have been conducted to verify the effectiveness of the gait generation algorithms. N foothold candidates for each leg have been used to search for the best tripod. For instance, if N=15, then N^3=3375, and these footholds are analyzed in less than 0.07 s using a Pentium III-based controller. This time is acceptable with regard to the sampling period of the controller (0.1 s). Note that increasing the number of foothold candidates, N, for each leg increases the computing time by N^3. The set of foothold candidates can be chosen taking into account the general features of the gait. For example, the subgroup used with crab angles of about 0° (forward motion) would differ from the subgroup used for crab angles of about 180° (backward motion). In general, N must be chosen as a trade-off between effectiveness and computation speed. The parameters used in the examples presented herein are: $SM_{\min} = 0.05\ \text{m}$, $H_1 = -0.13\ \text{m}$, $H_2 = -0.11\ \text{m}$, $H_3 = -0.20\ \text{m}$, $V_1 = 0.10\ \text{m/s}$, $V_2 = 0.30\ \text{m/s}$ and $V_3 = 0.10\ \text{m/s}$.

5.1. Simulation results

The first simulation example shows the algorithm's capability to maximize the maximum speed and the stability of the robot. Furthermore, it also shows how the variation of constant k_{ev} modifies the weight of these two properties.

Increasing the value of k_{ev} means giving a heavier weight to the absolute stability margin than to the reduced kinematic margin in the cost function, Ev. Fig. 8 represents the results obtained in this example for the values $k_{ev} \in [0,0.02,0.04,0.06,0.08,0.1]$. The value of k_{ev} is increased every 30 s. Fig. 8(a) and (b), respectively, show how the duration of the support and transfer phases decreases and the stability margin increases

as k_{ev} is increased. The minimum value of the reduced kinematic margin can also be observed to increase (see Fig. 8(c)). This is due to the shorter duration of the support phases, so the foot liftings take place before the reduced kinematic margin vanishes.

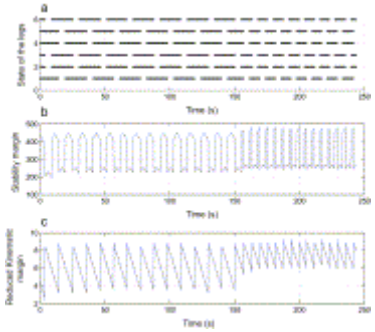

Full-size image (75K)

Fig. 8.

Gait measurements for different k_{ev}: (a) Time diagram: leg in support in solid line, otherwise leg in transfer; (b) Absolute stability margin; (c) Reduced kinematic margin.

In spite of the monotonous increasing of k_{ev}, there is no continuous evolution in either the variation of the absolute stability margin or the reduced kinematic margin, because the space has not been considered continuous in the foothold search — Only 15 possible discontinuous footholds for each leg are taken into account (see Section 3.3.3).

The second simulation example describes the algorithm's capacity to make the robot walk on terrain containing forbidden zones. These zones are generated randomly, and the robot travels in a straight line over them. The forbidden zones are drawn in black with a safe area in gray (see Fig. 9). The center of a foot can find support on the internal boundary of the safe areas, but never inside the forbidden zones. The footholds are represented by small circles. Fig. 9 depicts an overhead view of the terrain in which the forbidden zones and the footholds are drawn. Fig. 9(a) shows the results when the system performs the gait algorithm without taking into account the position of the forbidden zones. We can observe how the feet fall on forbidden zones in several cases. Fig. 9(b) plots the results when the algorithm takes into account the positions of the forbidden zones known a priori. In this case, we can see how all the robot's footholds lie outside the forbidden zones.

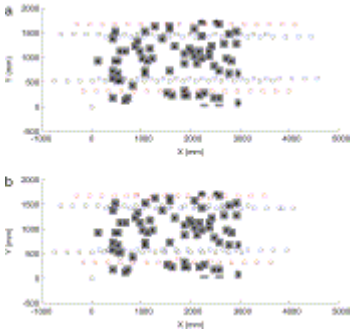
Full-size image (55K)

Fig. 9.

Footholds along a trajectory (small circles represent the footholds): (a) Footholds when the gait algorithm does not take the forbidden zones into account; (b) Footholds when the gait algorithm takes the forbidden zones into account.

The third simulation example illustrates how the algorithm can adapt to trajectory changes. This property is useful for accurate trajectory tracking. The test consists of observing the behavior of the gait when there is an abrupt change of the crab angle, from 0^{o} to 20^{o}. The robot walks parallel with the positive x axis, so the trajectories of the legs in support are straight lines along the negative x axis (see [Fig. 10], [Fig. 11], [Fig. 12], [Fig. 13] and [Fig. 14]).

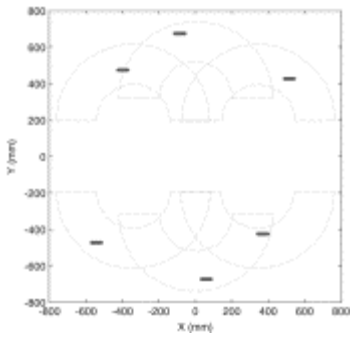
Full-size image (28K)

Fig. 10.

Crab angle change from 0^{o} to 20^{o} (State 1).

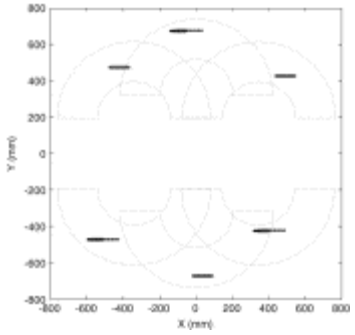

Full-size image (29K)

Fig. 11.

Crab angle change from 0^{o} to 20^{o} (State 2).

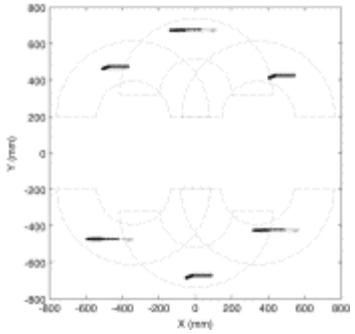

Full-size image (29K)

Fig. 12.

Crab angle change from 0^{o} to 20^{o} (State 3).

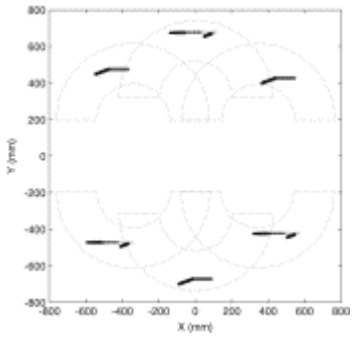

Full-size image (30K)

Fig. 13.

Crab angle change from 0^{o} to 20^{o} (State 4).

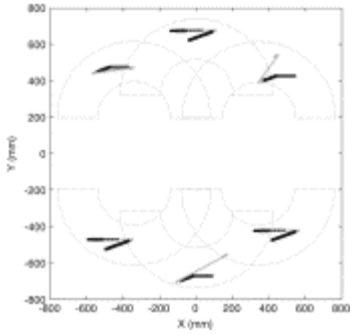

Full-size image (30K)

Fig. 14.

Crab angle change from 0 ° to 20 ° (State 5).

The correct operation of the crab gait is verified by representing the foothold of each leg in the body reference frame during a half locomotion cycle in [Fig. 10], [Fig. 11], [Fig. 12], [Fig. 13] and [Fig. 14]. The leg workspaces are indicated by discontinuous lines. The footholds of the legs in support are plotted in wide gray or dark gray dots, and the foot positions of the legs in transfer are plotted in small light gray or black dots.

In the first state (see Fig. 10), all legs are in support and the crab angle is null. The foothold trajectories are parallel with the positive x axis.

In the second state (see Fig. 11), tripod 2 (legs 2, 3 and 6) begins transfer and the crab angle is changed to 20 °. The footholds selected for tripod 2 are still adapted to the initial crab angle (0 °), since the transfer starts before the crab angle changes to 20 °. The trajectories of all legs are parallel with the positive x axis. Although a change in the crab angle has been commanded, the body continues moving along its x axis.

In the third state (see Fig. 12), tripod 2 (legs 2, 3 and 6) completes its transfer. The legs in support (legs 1, 4 and 5) adapt the direction of motion to 20 ° with respect to the x axis, and the body starts moving in the commanded direction.

In the fourth state (see Fig. 13), all the legs are in support, and the crab angle is 20 °. The footholds of each leg follow a trajectory such that the body continues moving with the specified crab angle.

In the fifth state (see Fig. 14), the transfer of tripod 1 (legs 1, 4 and 5) occurs. The footholds selected for the tripod in transfer adapt to the new crab angle, while the supporting footholds continue moving with the new crab angle.

The results show that the crab gait works correctly and is able to adapt to abrupt changes in the crab angle.

5.2. Experimental results

Finally, we performed some experiments to assess the gait algorithms using the real SILO-6 walking robot on terrain containing forbidden zones. This experiment was similar to the second simulation example described in Section 5.1.

The precise location of every forbidden zone was measured in advance with a DGPS. Therefore, the location of the forbidden zones was known before the robot went into motion. The forbidden zones were represented by black circles with a diameter of about 0.05 m (see Fig. 15). These circles were equivalent to the black squares in the second simulation. A black safe area with a diameter of about 0.15 m for each forbidden zone was also given. This was equivalent to the gray square in the second simulation (see Fig. 15). In our experiment, the robot avoided the forbidden zones perfectly throughout the traveled distance. This can be seen in the video available at [27]. This was just a preliminary experiment, because in real situations knowledge of the location of forbidden zones will be provided in real time by the scanning system composed of a mine detector and a scanning manipulator. See [8], [9], [26] and [27] for further details of the detecting device.


Full-size image (45K)

Fig. 15.

Experiment with the real SILO-6 walking robot traveling over forbidden zones (see video available at (SILO-6b) [27]).

6. Discussion and conclusions

This article presents the development of crab and turning gaits for hexapod robots on natural terrain characterized by containing uneven ground and forbidden zones. The algorithms are general for hexapod robots; however, both the geometrical model and the real prototype of the SILO-6 walking robot have been used for simulation and experimental purposes, respectively.

The main contribution of this work consists of the fact that the gait generation algorithms combine different features previously tested under ideal conditions. Thus, the proposed methods can adapt to irregular terrain, can work in the presence of forbidden zones and integrate crab and turning gaits that can be joined to perform trajectory tracking.

The gaits derived in this work have been devised for a real application, detecting and locating landmines in humanitarian demining missions. Hexapod robots are advisable for this particular application because of their high stability and speed. Additionally, a hexapod can achieve its highest speed by using alternating tripod gaits. Thus, our algorithms rely on a tripod gait, which normally performs periodic leg motions and takes periodic foothold positions. However, we have included a non-periodic feature to obtain a real free gait, which is based on heuristic rules capable of planning leg motions accurately and guaranteeing stability by using physical laws. These heuristic rules rely on the definition of foot-lifting instants and the computation of new footholds, and they are implemented by three modules: the foot-lifting planner, the body motion planner and the foothold planner. New concepts are provided in the definition of the reduced kinematic margin, the use of uncertainty in the estimation of the footholds and the criterion for foothold selection.

Several simulations and experiments have been conducted to assess the algorithms. These examples certify that the proposed gaits can maximize the robot's speed and stability, and they enable the robot to walk over terrain with forbidden zones as well. The gait algorithms have worked properly in a large number of experiments with a very low percentage of failures in finding leg and foothold sequences. This is mainly due to the convenient innate features of hexapod robots for finding stable sequences of footholds and leg motions. Additionally, simulations have been presented to illustrate how the algorithms can cope with sudden changes in the theoretical trajectory. Finally, some experiments have been discussed to illustrate the capability of the SILO-6 walking robot for adapting to irregular terrain and walking over forbidden zones. These experiments are available at [26] and [27]. The results have been assessed positively for a walking robot in humanitarian demining missions.

Acknowledgement

Funding for this paper was provided by CICYT under Grant DPI2001-1595 and DPI2004-05824.

References

[1] D. Catalbiano, G. Muscato, F. Russo, Localization and self calibration of a robot for volcano exploration, in: Proc. Int. Conf. Climbing and Walking Robots, New Orleans, LA, 2004, pp. 586–591.

[2] B. Gassmann, F. Zacharias, J.M. Zöllner, R. Dillmann, Localization of walking robots, in: Proceedings of the 2005 IEEE, International Conference on Robotics and Automation, Barcelona, Spain, 2005, pp. 1483–1488.

[3] J.A. Cobano, P. Gonzalez de Santos, J. Estremera, A new method to improve the localization of legged robots, in: Proc. Int. Conf. Climbing and Walking Robots, Brussels, Belgium, 2006, pp. 485–489.

[4] J.A. Cobano, J. Estremera and P. Gonzalez de Santos, Location of legged robots in outdoor environment, *Robotics and Autonomous Systems* **56** (2008), pp. 751–761.

[5] V. Kumar and K.J. Waldron, Adaptive gait control for a walking robot, *Journal of Robotic Systems* **6** (1989), pp. 49–75.

[6] M. Jimenez and P. Gonzalez de Santos, Terrain adaptive gait for walking machines, *The International Journal of Robotic Research* **16** (3) (1997), pp. 320–339. **Full Text** via CrossRef | View Record in Scopus | Cited By in Scopus (13)

[7] Q.J Huang and K. Nonami, Humanitarian mine detecting six-legged walking robot and hybrid neuro walking control with position/force control, *Mechatronics* **13** (2003), pp. 773–790. **Article** | PDF (620 K) | View Record in Scopus | Cited By in Scopus (21)

[8] P. Gonzalez de Santos, E. Garcia, J. Estremera and M.A. Armada, DYLEMA: Using walking robots for landmine detection and location, *International Journal of Systems Science* **36** (9) (2005), pp. 545–558. **Full Text** via CrossRef | View Record in Scopus | Cited By in Scopus (10)

[9] P. Gonzalez de Santos, J.A. Cobano, E. Garcia, J. Estremera and M.A. Armada, A six-legged-robot based system for humanitarian demining missions, *Mechatronics* **17** (2007), pp. 417–430. **Article** | PDF (1420 K) | View Record in Scopus | Cited By in Scopus (7)

[10] R.B. McGhee and A.A. Frank, On the stability properties of quadruped creeping gaits, *IEEE Transactions on Systems, Man and Cybernetics, SMC* **9** (4) (1968), pp. 176–182.

[11] A. Bessonov, N. Umnov, The analysis of gaits in six-legged vehicles according to their static stability, in: Proceedings of CISM-IFToMM Symposium on Theory and Practice of Robots and Manipulators, Udine, Italy, 1973, pp. 117–123.

[12] V.R. Kumar and K.J. Waldron, A review of research on walking vehicles. In: O. Khatib, J.J. Craig and T. Lozano-Perez, Editors, *The Robotics Review*, The MIT Press, Cambridge, Massachusetts (1989), pp. 243–266.

[13] E.I. Kugushev, V.S. Jaroshevskij, Problems of selecting a gait for a locomotion robot, in: Proceedings of the 4th International Joint Conference on Artificial Intelligence, Tiblisi, Georgia, URSS, 1975, pp. 789–793.

[14] R.B. McGhee and G.I. Iswandhi, Adaptive locomotion for a multilegged robot over rough terrain, *Mathematical Bioscience* **3** (1979), pp. 331–351.

[15] S. Hirose, A study of design and control of a quadruped walking robot, *The International Journal of Robotic Research* **10** (2) (1984), pp. 113–133. **Full Text** via CrossRef | View Record in Scopus | Cited By in Scopus (91)

[16] S. Bai, J. Low and T. Zielinska, Quadruped free gait generation based on the primary/secondary gait, *Robotica* **17** (1999), pp. 405–412. **Full Text** via CrossRef | View Record in Scopus | Cited By in Scopus (10)

[17] P. Pal and K. Jayarajan, Generation of free gaits a graph search approach, *IEEE Transaction on Robotics and Automation, RA* **7** (3) (1991), pp. 299–305. **Full Text** via CrossRef | View Record in Scopus | Cited By in Scopus (34)

[18] P. Pal and D. Kar, Gait optimization through search, *The International Journal of Robotic Research* **19** (4) (2000), pp. 394–408. **Full Text** via CrossRef | View Record in Scopus | Cited By in Scopus (2)

[19] D. Pack and H. Kang, Free gait control for a quadruped walking robot, *International Journal of Laboratory Robotics and Automation* **11** (2) (1999), pp. 71–81. View Record in Scopus | Cited By in Scopus (8)

[20] C. Eldershaw, M. Yim, Motion planning of legged vehicles in an unstructured environment, in: Proceedings of the International Conference on Robotics and Automation, Seoul, Korea, 2001, pp. 3383–3389. **Full Text** via CrossRef | View Record in Scopus | Cited By in Scopus (8)

[21] M. Lewis and Bekey, Gait adaptation in a quadruped robot, *Autonomous Robots* **12** (3) (2002), pp. 301–312. **Full Text** via CrossRef | View Record in Scopus | Cited By in Scopus (27)

[22] Y. Fukuoka, H. Kimura and A. Cohen, Adaptive dynamic walking of a quadruped robot on irregular terrain based on biological concepts, *The International Journal of Robotic Research* **22** (3–4) (2003), pp. 187–202. **Full Text** via CrossRef | View Record in Scopus | Cited By in Scopus (192)

[23] M.S. Erden and K. Leblebicioglu, Free gait generation with reinforcement learning for a six-legged robot Source, *Robotics and Autonomous Systems* **56** (3) (2008), pp. 199–212. **Article** | PDF (1662 K) | View Record in Scopus | Cited By in Scopus (8)

[24] J. Dean, T. Kindermann, J. Schmitz, M. Schumm and H. Cruse, Control of walking in the stick insect: From behavior and physiology to modeling, *Autonomous Robots* **7** (1999), pp. 271–288. **Full Text** via CrossRef | View Record in Scopus | Cited By in Scopus (17)

[25] F. Delcomyn, Walking robots and the central and peripheral control of locomotion in insects, *Autonomous Robots* **7** (1999), pp. 259–270. **Full Text** via CrossRef | View Record in Scopus | Cited By in Scopus (30)

[26] SILO-6. The SILO-6 and DYLEMA Projects' Home Page, 2009. Available at: http://www.iai.csic.es/users/silo6/.

[27] SILO-6. The SILO-6 and DYLEMA Videos, 2009. Available at: http://www.iai.csic.es/users/SILO6/SILO6_pics/forbiddenareas.wmv.

Corresponding author. Tel.: +34 918711900; fax: +34 918717050.

Vitae

J. Estremera received his B.E. degree in physics from the Complutense University of Madrid in 1998. In the same year, he joined the Industrial Automation Institute-CSIC, as a research assistant. In 2003 he received his Ph.D. from the Complutense University of Madrid. He has worked in a number of projects related with robotics, especially walking machines, in the Industrial Automation Institute-CSIC. He has participated in the design of the SILO4 quadruped and the SILO6 hexapod robots, being in charge of software design and development. In 2005 he joined the Robotic Locomotion Laboratory of Stanford University where he studied fast legged locomotion (running) under a post-doctoral research grant. In 2007 he joined the company GMV, where he works in the development of Satellite Based Augmentation Systems (EGNOS). His current research interests include fast legged locomotion, robot localization techniques and robotic exoskeletons.

J.A. Cobano received his degree in Physics from the University of Seville in 2001 and he joined the Institute of Industrial Automation (IAI-CSIC) in 2002. He received his Ph.D. Degree from the Complutense University of Madrid in 2007. His research topics include gait generation for legged robots, localization of mobile robots in outdoors and trajectory tracking. He was working as a visiting student at the University of Southern California (Los Angeles, USA) and Albert–Ludwigs-Universitat (Freibrug, Germany) where he developed algorithms for sensor integration and localization of mobile robots using odometry, dead-reckoning and extended Kalman-filter techniques. Currently, he is with the Robotics, Vision and Control Group of the Engineering School (University of Seville). His research interest includes control and autonomous navigation of aerial vehicles (UAV).

P. Gonzalez de Santos is a research scientist at the Institute of Industrial Automation (IAI) of the Spanish National Research Council (CSIC). He received his Ph.D. degree from the University of Valladolid, Spain. Since 1981, he has been involved actively in the design and development of industrial robots and also in special robotic systems. His work during last fifteen years has been focused to walking machines. He worked on the AMBLER project as a visiting scientist at the Robotics Institute of Carnegie Mellon University. Since then, he has been leading the development of several walking robots such as the RIMHO robot designed for intervention on hazardous environments, the ROWER walking machine developed for welding tasks in ship erection processes and the SILO4 walking robot intended for educational and basic research purposes. Dr. Gonzalez de Santos is now leading the DYLEMA project, which includes de construction of the SILO6 walking robot, to study how to apply walking machines to the field of humanitarian demining. He is currently the Head of the Department of Automatic Control at the IAI–CSIC.